IET Power Electronics

Research Article

IET Journals
The Institution of Engineering and Technology

Systematic approach to construct and assess power electronic conversion architectures using graph theory and its application in a fuel cell system

ISSN 1755-4535
Received on 26th October 2018
Revised 18th January 2019
Accepted on 15th February 2019
E-First on 11th March 2019
doi: 10.1049/iet-pel.2018.6143
www.ietdl.org

Wenping Zhang[1] ✉

[1]*Electrical and Computer Engineering Department, University of New Brunswick, Fredericton, Canada*
✉ *E-mail: wzhang18@unb.ca*

Abstract: With the proliferation of renewable energy generations, power conversion systems (PCSs) are becoming much more complex; it is becoming challenging to search all possible power conversion architectures (PCAs) and find the best optimisation in terms of different objectives. Therefore, this study investigates a systematic approach to construct and evaluate PCAs using graph theory. First, the components in PCSs are graphically modelled as either nodes or edges. Then, a generalised PCA deduction methodology is proposed, and all possible PCAs can be mathematically deduced by modifying elements in adjacency matrices. For a fuel cell (FC) generation system, 45 possible PCAs are found with the proposed method. Furthermore, an evaluation methodology based on graph theory is proposed. The performance indices of the deduced PCAs, including costs, efficiency, and reliability, are calculated. Then, an optimisation approach is applied to finding the best architecture compromise, where the one with the shortest distance to the ideal architecture is considered the best architecture compromise. For the FC demo system, with the proposed assessment methodology, the best architecture compromise (dc-bus structure) is found among 45 possible architectures. Finally, the experimental platform, which adopts the dc-bus optimised architecture, is built and experimental results validate the architecture selection.

1 Introduction

Power electronic (PE) techniques are playing a significant role in a range of applications, such as data centres, transportation systems, and renewable generations [1]. In the past few decades, numerous PE conversion architectures have been proposed to achieve various functions in different applications. Along with the advancement of PE technology, the goal of power conversion systems (PCSs) is more than just a voltage regulation. Furthermore, the objective of PCA design has been extended to (i) low costs, (ii) high output quality, (iii) high efficiency, (iv) high reliability and (v) low complexity [2]. Moreover, with the proliferation of renewable energy generations, the number of sources integrated into PCSs has significantly increased and the corresponding power conversion architectures (PCAs) are becoming much more complex. Consequently, it is becoming challenging to search all possible architectures for PCSs and find the optimised solution in terms of different objectives. Therefore, investigating a systematic approach to construct and evaluate PCAs is crucial, and attracting much attention among researchers.

Fig. 1 presents the PCAs reported in the past literature, where bus structures are dominant [3]. Based on the type of bus, the bus configurations can be classified into three categories: ac-bus, dc-bus and ac/dc bus hybrid [4]. Compared with ac-bus structures, dc-bus configurations become increasingly popular due to their merits, such as high reliability and scalability, easy control, and simple interface with renewables and energy storages [5]. Based on the number of dc-bus, the dc-bus structures can be further divided into two categories: singular-bus and multiple-bus. The singular-bus configurations can be unipolar or bipolar based on the polarity of the dc-bus [6]. For multiple-bus configurations, there are three types: parallel-, series-, and parallel/series-buses [7]. In addition, three types of non-bus structures are normally applied, including point-to-point, star- and ring-structures.

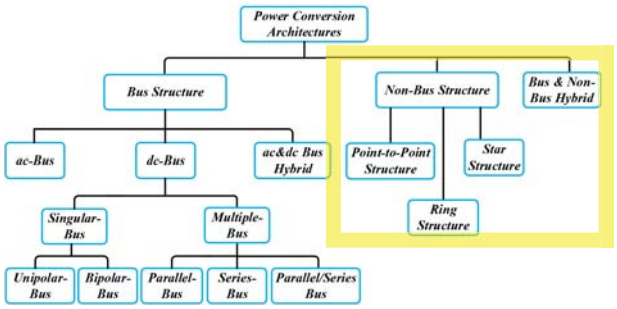

Fig. 1 *PE conversion architectures*

With respect to the PE system optimisation design, a number of papers propose different methods to construct and evaluate PCAs in term of costs, efficiency, reliability, and complexity. However, most of PCA construction methodologies reported are based on requirement analysis and topology enumerations. In [8], three multiple-input dc/dc architectures are compared in terms of costs, modularity, reliability, and flexibility. However, the analysis is relatively qualitative and the characteristics of input sources are not considered. In [9], Li *et al.* investigate PCAs for FC generation systems and the efficiency performance for four different PCAs is evaluated. Since the costs of FCs are high, maximising system efficiency becomes a top priority. In [10], a multi-source uninterruptible power supply (UPS) system is proposed to boost system reliability. Furthermore, four power conversion structures are enumerated and compared in terms of reliability. Shi *et al.* further propose a graphical methodology to deduce possible architectures for multi-source UPS systems, which is based on a simplified component model [11]. Moreover, the deduced architectures in [11], including star, bus, ring, and hybrid structures, are evaluated in terms of reliability. However, there is a lack of rigid mathematical deductions, and the proposed method is a graphical enumeration in essence. Similar methodologies are applied in microgrids and several papers address how PE configurations can affect the reliability of microgrids [12, 13]. Overall, the majority of methodologies reported in the past literature are PCA enumerations, which can only be suitable for specific applications. Also, most of the optimisations reported are single objective rather than multiple objectives.

© The Institution of Engineering and Technology 2019

EXHIBIT
2016
Page Page 1 of 11 (IPR2023-00758)
Netflix, Inc. v. GoTV Streaming, LLC

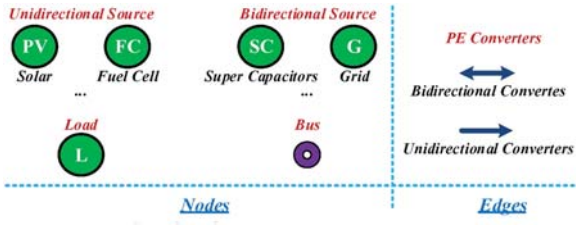

Fig. 2 *Graphical modelling for five types of components*

Presently, multiple-objective optimisation in power electronics can be found in power converter design. The common objectives include power density, efficiency, reliability, and costs. There are two main multi-objective optimisation methods reported [14]. The first one is called aggregate function approaches, which weigh different objective functions into a single objective function. This method presents the relative importance of the objectives by allocating different weighing factors. Thus, it is not suitable when the relative relationship of the objectives is unknown [14]. The second one is called the Pareto front (PF) techniques. Compared with the first method, this method does not weigh the objectives beforehand. To achieve PF techniques, there are three common algorithms: (i) heuristic genetic/evolutionary algorithms [14], (ii) algorithms with guaranteed convergence to the Pareto optimal solution [15], and (iii) iterative grid search algorithms with an appropriate discretisation of the variables [16, 17]. Among these three algorithms, the first algorithm cannot always guarantee to find optimal solutions, and thus the two latter approaches are more commonly adopted. Furthermore, due to the merits of numerical robustness and simplicity of implementation, the grid search algorithm is becoming more popular. Also, the grid search algorithm is often considered as systematical enumerations. In [18], a life cycle cost driven optimisation process is implemented with enumeration algorithms. By sweeping over a range of switching frequencies, the optimal components for the converters, such as switches, inductors, transformers etc., are found. For multiple boundary conditions, the concept of the design space (DS) is considered promising, and it has been applied to optimise output filters in PE converters [19]. Furthermore, Boillat *et al*. [20] combine the DS analysis and PF optimisation to design output filters in cases of six combined requirements. Another aspect of multi-objective optimisations that researchers are focusing on is improving the system evaluation models regarding efficiency, power density, and costs. For instance, thermal models for semiconductors and magnetics are added in [21–23] to improve the accuracy of the converter model during dynamic operations. In [24], the cost models for each component are detailed and numerical values for the parameters are considered. Furthermore, advanced and experimentally verified loss and thermal models are incorporated to improve the accuracy of the dynamic model. In addition, several papers address the sensitivity of the optimal solutions, such as the impact of parameter variations.

Graph theory started in the 17th century when Euler solved the famous problem: 'Seven bridges of Konigsberg'. Presently, it has been applied in various engineering fields, such as computer science, networking, and power systems [25]. For power systems, the graph theory is mainly applied in three directions: system operation analysis, design of power system network, and system reconfigurations after faults. Specifically, in [26], graph theory is used to analyse load flow and loss allocation in a power system, which can monitor the system operation status and find overloaded buses. In [27], graph theory is applied to design optimal placement for phasor measurement units in a power system. Garg *et al.* apply graph theory to optimise and evaluate power plant selections [28]. Furthermore, graph theory is applied to reconfigure power networks in cases of faulty or overloaded conditions [29], where less loaded paths are chosen among the feasible candidates. However, there are a limited number of papers that apply graph theory in power electronics. Smedley and Cuk develop a unified graphical modelling approach called 'switching flow graph' to study non-linear dynamic behaviours of pulse-width-modulated converters [30]. In [31], the phenomenon of sneak paths in PE converters is investigated using graph theory and the design to eliminate sneak paths is proposed as well. Overall, there are not many papers reported to use graph theory to deduce and evaluate PCAs yet.

Therefore, this study will investigate a systematic approach to construct and evaluate PCAs using graph theory. The main features of the proposed methodology are as follows:

i. The proposed methodology of searching possible PCAs is a systematic approach. All possible PCAs can be mathematically found with the proposed method. Also, it can be applied in any complex systems with any number of nodes (sources and loads).
ii. The proposed methodology of assessing PCAs is also based on graph theory. It is a generalised scenario, and the performance indices can be mathematically obtained with graph theory. Also, a multi-objective optimisation of finding the shortest distance to the ideal architecture is proposed. It is easy to find the best PCA compromise among all possible PCAs.
iii. The proposed method is based on a mathematical deduction and can be easily implemented via software computing. This makes possible to find the optimised PCAs for large-scale PCSs with the aid of computers.

2 Component modelling for PCSs

The components in a PCS can be divided into five categories, including (i) unidirectional sources, such as solar panels and fuel cells, which can only release power, (ii) bidirectional sources, such as the grid and supercapacitors (SCs), which can both release and absorb power, (iii) loads, (iv) PE converters, and (v) power distribution buses. To investigate possible PCAs using graph theory, these five types of components are modelled as either nodes or edges as shown in Fig. 2. Three points are made here.

i. The unidirectional and bidirectional sources, loads, and buses are modelled as nodes; PE converters are modelled as edges. The symbol of the buses is different in Fig. 2, and the main purpose is to differentiate the buses with other nodes (sources and loads).
ii. The bidirectional edge represents bidirectional converters, while the unidirectional edge represents unidirectional converters. Also, the direction of the edge can denote the power flow direction of the converter.
iii. For power distribution buses, the number of PE converters connected to them should be at least three.

By applying the graphical models, a PCS can be transformed into a graph. Then, the problem of searching for possible PCAs can be transformed into a graph issue. Fig. 3*a* presents an example, where a FC generation system is physically transformed into a graph.

In the FC system, the system can be operated in either grid-connected mode or stand-alone mode. Note that the SC is applied to provide dynamic power when the output power steps up or down as shown in Fig. 3*b*. This can compensate for the slow dynamics of FCs and prolong their lifespan [32].

The following sections will propose a PCA constructing approach based on graph theory. Meanwhile, the FC generation system is introduced to demonstrate the approach.

3 Non-bus PCA construction

This section presents the method of constructing non-bus PCAs.

3.1 Obtain possible graphs by modifying adjacency matrices

First, list all nodes in the system. In the demo system (see Fig. 4*a*), there are three nodes, including fuel cell (FC), SC and ac grid/load (G/L). Then, add edges to connect these nodes and obtain possible graphs, and this can be completed based on adjacency matrices.

© The Institution of Engineering and Technology 2019

Page Page 2 of 11 (IPR2023-00758)
Netflix, Inc. v. GoTV Streaming, LLC

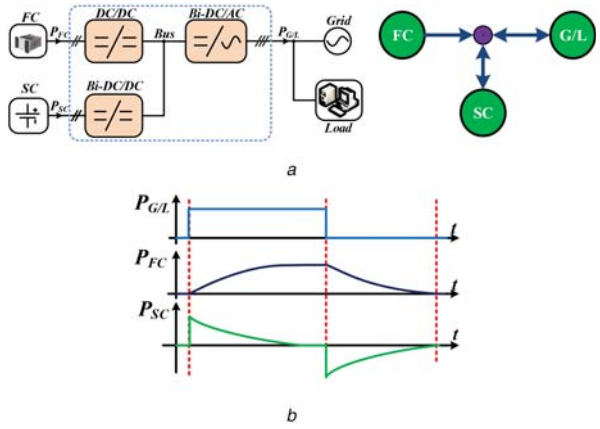

Fig. 3 *FC generation system*
(a) Graphical model for a FC generation system, ***(b)*** SC compensates FC's slow dynamics

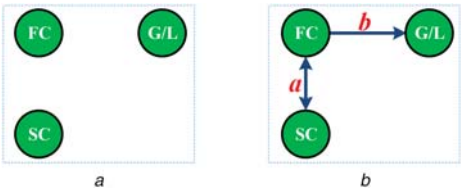

Fig. 4 *Graph of FC generation demo system*
(a) Three nodes, ***(b)*** Graph after adding edges

Table 1 26 modified adjacency matrices

Number of modified elements	Modified adjacency matrices *A*
2	$\begin{bmatrix}0&a&b\\0&0&0\\0&0&0\end{bmatrix}, \begin{bmatrix}0&a&0\\a&0&0\\0&0&0\end{bmatrix}, \begin{bmatrix}0&a&0\\0&0&c\\0&0&0\end{bmatrix}, \begin{bmatrix}0&a&0\\0&0&0\\0&c&0\end{bmatrix}, \begin{bmatrix}0&0&b\\a&0&0\\0&0&0\end{bmatrix}, \begin{bmatrix}0&0&b\\0&0&c\\0&0&0\end{bmatrix}, \begin{bmatrix}0&0&b\\0&0&0\\0&c&0\end{bmatrix}, \begin{bmatrix}0&0&0\\a&0&c\\0&0&0\end{bmatrix}, \begin{bmatrix}0&0&0\\a&0&0\\0&c&0\end{bmatrix}, \begin{bmatrix}0&0&0\\0&0&c\\0&c&0\end{bmatrix}$
3	$\begin{bmatrix}0&0&0\\a&0&c\\0&c&0\end{bmatrix}, \begin{bmatrix}0&0&b\\0&0&c\\0&c&0\end{bmatrix}, \begin{bmatrix}0&0&b\\a&0&0\\0&c&0\end{bmatrix}, \begin{bmatrix}0&0&b\\a&0&c\\0&0&0\end{bmatrix}, \begin{bmatrix}0&a&0\\0&0&c\\0&c&0\end{bmatrix}, \begin{bmatrix}0&a&0\\a&0&0\\0&c&0\end{bmatrix}, \begin{bmatrix}0&a&0\\a&0&c\\0&0&0\end{bmatrix}, \begin{bmatrix}0&a&b\\0&0&0\\0&c&0\end{bmatrix}, \begin{bmatrix}0&a&b\\0&0&c\\0&0&0\end{bmatrix}, \begin{bmatrix}0&a&b\\a&0&0\\0&0&0\end{bmatrix}$
4	$\begin{bmatrix}0&0&b\\a&0&c\\0&c&0\end{bmatrix}, \begin{bmatrix}0&a&0\\a&0&c\\0&c&0\end{bmatrix}, \begin{bmatrix}0&a&b\\0&0&c\\0&c&0\end{bmatrix}, \begin{bmatrix}0&a&b\\a&0&0\\0&c&0\end{bmatrix}, \begin{bmatrix}0&a&b\\a&0&c\\0&0&0\end{bmatrix}$
5	$\begin{bmatrix}0&a&b\\a&0&c\\0&c&0\end{bmatrix}$

For the demo system as shown in Fig. 4*a*, the adjacency matrix $\boldsymbol{A}$ is shown in (1), where the ordering of three nodes is assumed to be FC, SC and G/L

$$\boldsymbol{A} = \begin{array}{c} \\ \text{FC} \\ \text{SC} \\ \text{G/L} \end{array} \begin{array}{c} \begin{array}{ccc} \text{FC} & \text{SC} & \text{G/L} \end{array} \\ \begin{bmatrix}0&0&0\\0&0&0\\0&0&0\end{bmatrix} \end{array}. \tag{1}$$

Based on the graph theory, if an element in the adjacency matrix is modified to non-zero, an edge can be added correspondingly. For instance, if the element (FC, G/L) in $\boldsymbol{A}$ is changed to '*b*' as shown in (2), a unidirectional edge *b* is added from FC to G/L in the graph as shown in Fig. 4*b*. Similarly, if the symmetry elements (FC, SC) and (SC, FC) are both modified to '*a*', a bidirectional edge *a* is added between FC and SC in the graph as shown in Fig. 4*b*

$$\boldsymbol{A}' = \begin{array}{c} \\ \text{FC} \\ \text{SC} \\ \text{G/L} \end{array} \begin{array}{c} \begin{array}{ccc} \text{FC} & \text{SC} & \text{G/L} \end{array} \\ \begin{bmatrix}0&a&b\\a&0&0\\0&0&0\end{bmatrix} \end{array}. \tag{2}$$

Therefore, by modifying the elements in the adjacency matrix, new graphs can be deduced. Note that three assumptions are made while modifying the elements.

i. The elements in the main diagonal are maintained as '0'. The fact is that self-loops will be generated if these elements are changed to non-zero. However, these created self-loops are meaningless for power conversions.
ii. The element (G/L, FC) is maintained as '0', and thus the route from the G/L to FC is not considered. The reason is that FC in the system only outputs power and cannot absorb the main power from the G/L side.
iii. Parallel edges are not considered. For instance, if multiple converters are directly connected in parallel for redundancy, parallel edges will occur in the graph. However, this case will not be considered in this study.

With these two assumptions, there are five elements in the adjacency matrix that are allowed to be modified. As shown in (3), these five elements are boxed.

$$\boldsymbol{A} = \begin{bmatrix}0&\boxed{0}&\boxed{0}\\\boxed{0}&0&\boxed{0}\\0&\boxed{0}&0\end{bmatrix}. \tag{3}$$

Since there are five elements that can be modified, the total number of adjacency matrices that can be obtained after the modification is shown in (4). Note that, to connect three nodes in the graph, the number of the elements selected to modify is at least two

$$N_1 = \sum_{k=2}^{N_m} C_{N_m}^k = C_5^2 + C_5^3 + C_5^4 + C_5^5 = 26. \tag{4}$$

where N_m is the total number of elements in the adjacency matrix that can be modified and $N_m = 5$ here.

Table 1 presents these 26 modified adjacency matrices. The numbers marked in red indicate that the corresponding elements are modified.

3.2 Find the graphs which meet the system's basic requirements among all possible graphs

From above, 26 possible graphs are deduced. Then, check if these graphs can meet the basic requirements of the system. In the demo system, the basic requirements are as follows:

i. The FC needs to feed the G/L as shown in Fig. 5*a*.
ii. The SC needs are charged from the FC as shown in Fig. 5*b*.
iii. The dynamic responses of FCs are slow. To compensate the FC's slow dynamics, SCs should be able to charge and discharge dynamic power. Note that the SC can charge and

© The Institution of Engineering and Technology 2019
Page Page 3 of 11 (IPR2023-00758)
Netflix, Inc. v. GoTV Streaming, LLC

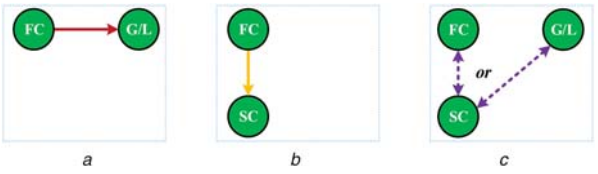

Fig. 5 *Requirement analysis for the FC demo system*
(a) Requirement 1, ***(b)*** Requirement 2, ***(c)*** Requirement 3

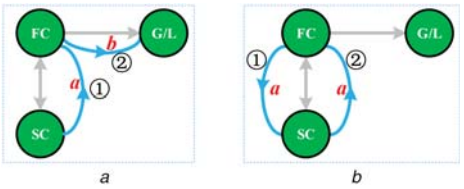

Fig. 6 *2-edge walks in the demo graph*
(a) 2-edge walk from SC to G, ***(b)*** Invalid 2-edge walk

discharge the power either to the FC directly or to the G/L as shown in Fig. 5*c*. In either way, the power change rate of the FC can be restrained.

Therefore, based on three above requirements, check if these paths, including from FC to G/L, from FC to SC and from SC to FC (or to G/L), are created in the deduced graphs. The approach of checking those paths with graph theory is detailed as follows.

Taking the adjacency matrix in (2) as an example, the square of $\boldsymbol{A}'$ is obtained as shown in (5)

$$(\boldsymbol{A}')^2 = \begin{bmatrix} a^2 & 0 & 0 \\ 0 & a^2 & ab \\ 0 & 0 & 0 \end{bmatrix}. \tag{5}$$

Based on graph theory, the elements in $(\boldsymbol{A}')^2$ represent the corresponding two-walk paths in the graph. For instance, the element (SC, G/L) is ab. This means there is a two-walk path from SC to G/L, which is via edges a and b. This two-walk path can be found in the graph (see Fig. 6*a*).

It is worth pointing out that the elements having a^2, b^2, and c^2 indicate that the corresponding paths walk the same edges twice. For instance, the element (FC, FC) is a^2, and thus there is a path that FC goes back to itself after walking through the bidirectional edge a twice (see Fig. 6*b*). However, this is not valid in practice, since an edge (a converter) can only be used once in one path. Therefore, the paths, which have a^2, b^2, and c^2, should be removed. Then, the matrix is updated and presented in (6)

$$(\boldsymbol{A}')^2 = \begin{bmatrix} 0 & 0 & 0 \\ 0 & 0 & ab \\ 0 & 0 & 0 \end{bmatrix}. \tag{6}$$

Based on graph theory, all the paths in the graph can be found in the sum of the adjacency matrix powers, as shown in (7). The matrix $\boldsymbol{A}'_{\mathrm{T}}$ is also called the path matrix

$$\boldsymbol{A}'_{\mathrm{T}} = \sum_{k=1}^{N-1} (\boldsymbol{A}')^k = \boldsymbol{A}' + (\boldsymbol{A}')^2 = \begin{bmatrix} 0 & a & b \\ a & 0 & ab \\ 0 & 0 & 0 \end{bmatrix}, \tag{7}$$

where N is the total number of nodes in the graph.

From (7), there are four paths in the graph and these four paths are presented in Table 2. From it, the basic paths, including from FC to G/L, from FC to SC and from SC to FC (or G/L), are created in this graph. Therefore, the basic requirements of the system can be met.

Following the same method, the path matrices for all 26 graphs are calculated and presented in Fig. 7. Note that the numbers

Table 2 Four paths in the graph A'

Elements	Paths	Walking edges	Functions
(FC, G/L): b	FC → G/L	edge *b*	FC powers G/L
(FC, SC): a	FC → SC	edge *a*	FC charges SC
(SC, FC): a	SC → FC	edge *a*	SC discharges to FC
(SC, G/L): ab	SC → G/L	edges *a* and *b*	SC discharges to G/L

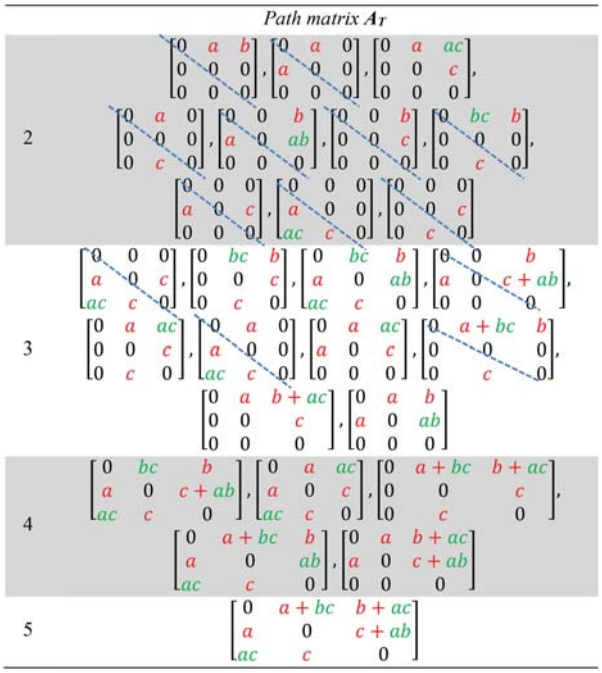

Fig. 7 *Path matrices for all 26 possible graphs*

marked in red indicate one-walk paths, and the numbers in green show two-walk paths.

Based on the path matrices, check if the corresponding graphs meet the requirement of the system. Specifically, check if the following paths are created: from FC to G/L, from FC to SC and from SC to FC (or to G/L). If not, this graph cannot meet the requirement and should be eliminated. As a result, 13 unqualified graphs are found and these graphs are crossed out as shown in Fig. 7. Therefore, there are only 13 qualified graphs left.

Since the main task of the system is to send FC's power to the G/L side, the element (FC, G/L) in the path matrix is the most concerning. From the path matrices in Fig. 7, these 13 qualified graphs can be divided into three categories based on the element (FC, G/L), which are shown in Table 3.

In category I, the element (FC, G/L) is 'ac', which means the FC powers the G/L via two edges (a and c). Therefore, the system efficiency from FC to the G/L side is relatively low. In category II, the element (FC, G/L) is 'b', which means the FC powers the G/L via edge b and the system efficiency is higher than the first category. In category III, the element (FC, G/L) is '$b + ac$', which means the FC can power the G/L either via edge b or via edges a and c. Therefore, the redundancy is created and the reliability of the FC powering the G/L is enhanced as well.

Based on Tables 1 and 3, these qualified graphs are plotted as shown in Fig. 8.

4 Singular-bus PCA construction

This section will present the method of constructing singular-bus PCAs. For the FC demo system, a power bus is added. Note that the added bus could be a dc bus or an ac bus, and this study will focus on dc bus PCAs.

First, list all nodes in the system. As shown in Fig. 9*a*, there are four nodes, which are FC, SC, G/L, and bus. Then, based on the

IET Power Electron., 2019, Vol. 12 Iss. 6, pp. 1499-1509
© The Institution of Engineering and Technology 2019

Page Page 4 of 11 (IPR2023-00758)
Netflix, Inc. v. GoTV Streaming, LLC

Table 3 Three categories based on the element (FC, G/L)

	Path matrix $\boldsymbol{A}_T$
I	$\begin{bmatrix}0 & a & ac\\0 & 0 & c\\0 & 0 & 0\end{bmatrix}, \begin{bmatrix}0 & a & ac\\0 & 0 & c\\0 & c & 0\end{bmatrix}, \begin{bmatrix}0 & a & ac\\a & 0 & c\\0 & 0 & 0\end{bmatrix}, \begin{bmatrix}0 & a & ac\\a & 0 & c\\ac & c & 0\end{bmatrix}$
II	$\begin{bmatrix}0 & bc & b\\0 & 0 & c\\0 & c & 0\end{bmatrix}, \begin{bmatrix}0 & bc & b\\a & 0 & ab\\ac & c & 0\end{bmatrix}, \begin{bmatrix}0 & bc & b\\a & 0 & c+ab\\ac & c & 0\end{bmatrix}, \begin{bmatrix}0 & a & b\\a & 0 & ab\\0 & 0 & 0\end{bmatrix}$ $\begin{bmatrix}0 & a+bc & b\\a & 0 & ab\\ac & c & 0\end{bmatrix}$
III	$\begin{bmatrix}0 & a & b+ac\\0 & 0 & c\\0 & 0 & 0\end{bmatrix}, \begin{bmatrix}0 & a+bc & b+ac\\0 & 0 & c\\0 & c & 0\end{bmatrix}, \begin{bmatrix}0 & a & b+ac\\a & 0 & c+ab\\0 & 0 & 0\end{bmatrix},$ $\begin{bmatrix}0 & a+bc & b+ac\\a & 0 & c+ab\\ac & c & 0\end{bmatrix}$

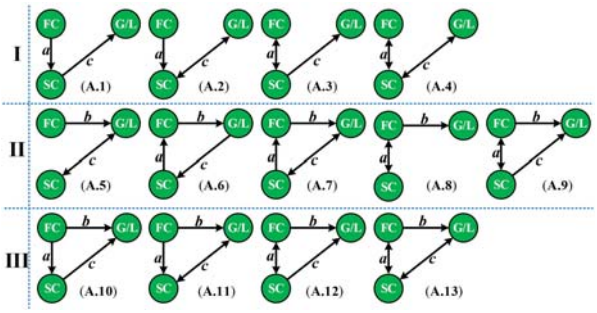

Fig. 8 *Three types of the qualified graphs for the demo system*

adjacency matrix, add edges to connect the nodes and obtain possible graphs.

For the demo system as shown in Fig. 9*a*, the adjacency matrix $\boldsymbol{A}$ is shown in (8), where the ordering of four nodes is assumed to be FC, SC, G/L, and bus

$$\boldsymbol{A} = \begin{array}{c} \\ \text{FC} \\ \text{SC} \\ \text{G/L} \\ \text{Bus} \end{array} \begin{array}{c} \begin{array}{cccc} \text{FC} & \text{SC} & \text{G/L} & \end{array} \\ \begin{bmatrix}0 & 0 & 0 & 0\\0 & 0 & 0 & 0\\0 & 0 & 0 & 0\\0 & 0 & 0 & 0\end{bmatrix} \end{array}. \tag{8}$$

Then, modify the elements in the adjacency matrix to non-zero and deduce new graphs. Several assumptions are made while modifying the elements

i. The elements in the main diagonal are maintained as '0'.
ii. The number of edges connected to the bus is at least three. Therefore, three nodes (FC, SC, and G/L) all have to be connected to node-*bus* as shown in Fig. 9*b*.
iii. The elements (G/L, FC) and (bus, FC) are maintained as '0'. The reason is that FCs cannot absorb the main power. Thus, edge *a* between FC and the bus is unidirectional.
iv. Edge *c* from the bus to the G/L indicates a dc/ac inverter. Presently, the inverters are normally bidirectional, and thus edge *c* is considered bidirectional here.
v. The edge between the SC and the bus (edge *b*) can be either unidirectional or bidirectional as shown in Fig. 9*b*.

First, edge *b* is assumed to be bidirectional and the following analysis method can be also applied the case where the edge *b* is unidirectional. With the above assumptions, there are five elements in the adjacency matrix that are allowed to be modified. As shown in (9), these five elements are boxed

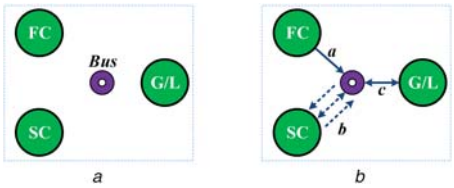

Fig. 9 *Single-bus graph for FC generation demo system*
(a) Four nodes, ***(b)*** Assumptions

$$\boldsymbol{A} = \begin{bmatrix}0 & \boxed{0} & \boxed{0} & a\\ \boxed{0} & 0 & \boxed{0} & b\\0 & \boxed{0} & 0 & c\\0 & b & c & 0\end{bmatrix}. \tag{9}$$

Since there are five elements that can be modified, the total number of adjacency matrices that can be obtained after the modifications is shown (10)

$$N_2 = \sum_{k=0}^{5} C_5^k = C_5^0 + C_5^1 + C_5^2 + C_5^3 + C_5^4 + C_5^5 = 32. \tag{10}$$

Table 4 presents these 32 adjacency matrices. The numbers marked in red indicate that the corresponding elements are modified.

Furthermore, the path matrix for each graph can be found with (11)

$$\boldsymbol{A}_T = \sum_{k=1}^{N-1} (\boldsymbol{A})^k = \boldsymbol{A} + (\boldsymbol{A})^2 + (\boldsymbol{A})^3, \tag{11}$$

where N is the total number of nodes in the graph.

Therefore, substitute the adjacency matrices in Table 4 into (11); the corresponding path matrices can be obtained. Based on the path matrices, check if the corresponding graphs meet the requirement of the system. An example is shown in (12).

$$\boldsymbol{A} = \begin{bmatrix}0 & d & e & a\\0 & 0 & 0 & b\\0 & 0 & 0 & c\\0 & b & c & 0\end{bmatrix},$$
$$A_T = \begin{bmatrix}0 & d+ab+bce & e+ac+bcd & a+ce+bd\\0 & 0 & bc & b\\0 & bc & 0 & c\\0 & b & c & 0\end{bmatrix}. \tag{12}$$

From it, the basic paths, including from FC to G/L, from FC to SC and from SC to FC (or G/L), are created in this graph. Therefore, the basic requirements of the system can be met. As is mentioned above, the element (FC, G/L) is the most concerning. From (12), there are three paths from the FC to the G/L generated, which are respectively via edge *e*, via edges *a* and *c*, and via edges *d*, *b* and *c*. Therefore, the reliability of the FC powering the G/L is enhanced. Also, these three paths can be found in the graph (see Fig. 10).

Following the same method, the path matrices for all 32 graphs are calculated. Then, based on the number of paths from the FC to the G/L, these 32 deduced graphs can be divided into five categories. These five types of singular-bus graphs are plotted in Fig. 11.

In category I, there is only one path from the FC to the G/L, which is via edges *a* and *c*. In category II, there are two paths from the FC to the G/L. One path is via edges *a* and *c*, and the other path is either via edges *a*, *b* and *f* or via edges *d*, *b,* and *c* or via edge *e*. In category III, there are three paths from the FC to the G/L. One path is via edge *e*. The second path is via edges *a* and *c*. The third path is either via edges *a*, *b*, and *f* or via edges *d*, *b,* and *c*. In category IV, there are four paths from the FC to the G/L, which are via edges *a* and *c*, via edges *d*, *b* and *c*, via edges *d* and *f*, and via edges *a*, *b* and *f*. In category V, there is one more path added (via

© The Institution of Engineering and Technology 2019
Page Page 5 of 11 (IPR2023-00758)
Netflix, Inc. v. GoTV Streaming, LLC

Table 4 32 modified adjacency matrices

	Modified adjacency matrices $\boldsymbol{A}$
0	$\begin{bmatrix}0&0&0&a\\0&0&0&b\\0&0&0&c\\0&b&c&0\end{bmatrix}$
1	$\begin{bmatrix}0&d&0&a\\0&0&0&b\\0&0&0&c\\0&b&c&0\end{bmatrix}, \begin{bmatrix}0&0&e&a\\0&0&0&b\\0&0&0&c\\0&b&c&0\end{bmatrix}, \begin{bmatrix}0&0&0&a\\d&0&0&b\\0&0&0&c\\0&b&c&0\end{bmatrix}, \begin{bmatrix}0&0&0&a\\0&0&f&b\\0&0&0&c\\0&b&c&0\end{bmatrix}, \begin{bmatrix}0&0&0&a\\0&0&0&b\\0&f&0&c\\0&b&c&0\end{bmatrix}$
2	$\begin{bmatrix}0&d&e&a\\0&0&0&b\\0&0&0&c\\0&b&c&0\end{bmatrix}, \begin{bmatrix}0&d&0&a\\d&0&0&b\\0&0&0&c\\0&b&c&0\end{bmatrix}, \begin{bmatrix}0&d&0&a\\0&0&f&b\\0&0&0&c\\0&b&c&0\end{bmatrix}, \begin{bmatrix}0&d&0&a\\0&0&0&b\\0&f&0&c\\0&b&c&0\end{bmatrix}, \begin{bmatrix}0&0&e&a\\0&0&0&b\\0&f&0&c\\0&b&c&0\end{bmatrix}, \begin{bmatrix}0&0&e&a\\d&0&0&b\\0&f&0&c\\0&b&c&0\end{bmatrix}, \begin{bmatrix}0&0&0&a\\d&0&f&b\\0&0&0&c\\0&b&c&0\end{bmatrix}, \begin{bmatrix}0&0&0&a\\d&0&0&b\\0&f&0&c\\0&b&c&0\end{bmatrix}, \begin{bmatrix}0&0&0&a\\0&0&f&b\\0&f&0&c\\0&b&c&0\end{bmatrix}$
3	$\begin{bmatrix}0&d&e&a\\d&0&0&b\\0&0&0&c\\0&b&c&0\end{bmatrix}, \begin{bmatrix}0&d&e&a\\0&0&f&b\\0&0&0&c\\0&b&c&0\end{bmatrix}, \begin{bmatrix}0&d&e&a\\0&0&0&b\\0&f&0&c\\0&b&c&0\end{bmatrix}, \begin{bmatrix}0&d&0&a\\d&0&f&b\\0&0&0&c\\0&b&c&0\end{bmatrix}, \begin{bmatrix}0&d&0&a\\d&0&0&b\\0&f&0&c\\0&b&c&0\end{bmatrix}, \begin{bmatrix}0&d&0&a\\0&0&f&b\\0&f&0&c\\0&b&c&0\end{bmatrix}, \begin{bmatrix}0&0&e&a\\d&0&f&b\\0&0&0&c\\0&b&c&0\end{bmatrix}, \begin{bmatrix}0&0&e&a\\d&0&0&b\\0&f&0&c\\0&b&c&0\end{bmatrix}, \begin{bmatrix}0&0&0&a\\d&0&f&b\\0&f&0&c\\0&b&c&0\end{bmatrix}$
4	$\begin{bmatrix}0&d&e&a\\d&0&f&b\\0&0&0&c\\0&b&c&0\end{bmatrix}, \begin{bmatrix}0&d&e&a\\d&0&0&b\\0&f&0&c\\0&b&c&0\end{bmatrix}, \begin{bmatrix}0&d&e&a\\0&0&f&b\\0&f&0&c\\0&b&c&0\end{bmatrix}, \begin{bmatrix}0&d&0&a\\d&0&f&b\\0&f&0&c\\0&b&c&0\end{bmatrix}, \begin{bmatrix}0&0&e&a\\d&0&f&b\\0&f&0&c\\0&b&c&0\end{bmatrix}$
5	$\begin{bmatrix}0&d&e&a\\d&0&f&b\\0&f&0&c\\0&b&c&0\end{bmatrix}$

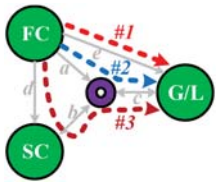

Fig. 10 *Three paths from FC to the G/L*

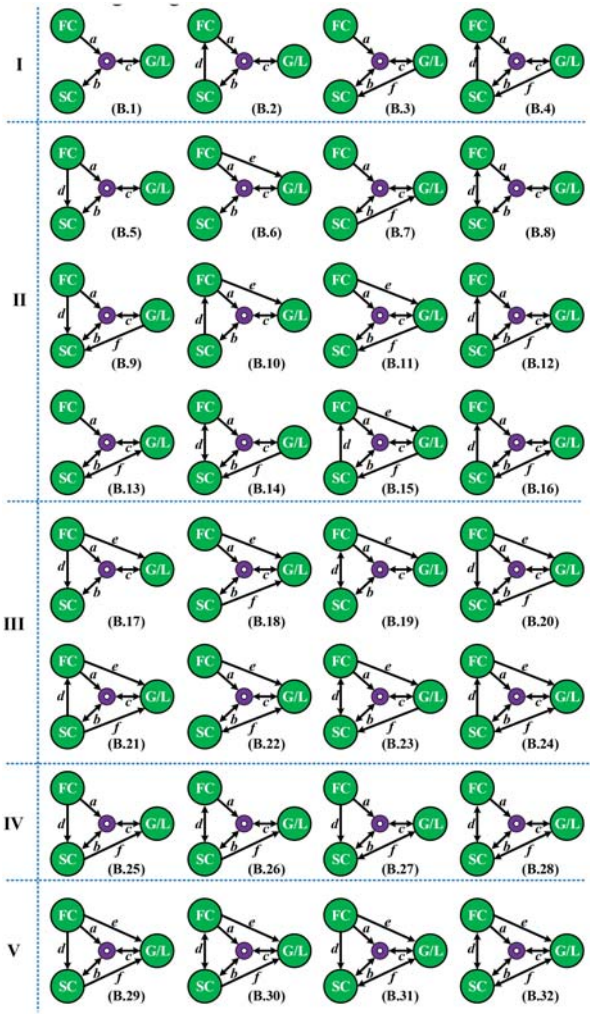

Fig. 11 *Five types of the singular-bus graphs*

edge *e*) compared with the paths in category IV. Generally, the higher the number of the created paths from the FC to the G/L is, the higher the reliability of FC powering the G/L is.

The same approach can be extended to multiple-bus structures. However, multiple-bus structures are relatively complex for three-node systems, and thus will not be elaborated in this study.

5 Assessment on the deduced PCAs

In this section, the deduced architectures will be evaluated in terms of costs, efficiency, and reliability.

5.1 System parameters

The system parameters for the case study are presented in Table 5.

Based on the system parameters, the topologies selected for the evaluation are presented in Fig. 12. The non-isolated topologies are selected since they can bring higher efficiency for the system.

Table 6 gives the converter selections for different edges in the graphs.

IET Power Electron., 2019, Vol. 12 Iss. 6, pp. 1499-1509
© The Institution of Engineering and Technology 2019

Page Page 6 of 11 (IPR2023-00758)
Netflix, Inc. v. GoTV Streaming, LLC

	1: Unidirectional dc/dc	2: Bidirectional dc/dc
topology	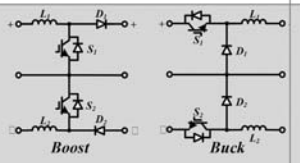	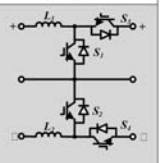
cost (×$500)	C_1=1	C_2=1.2
efficiency	η_1=0.97	η_2=0.97
reliability	$R_1 = e^{-6\times10^{-6}t}$	$R_2 = e^{-12\times10^{-6}t}$
	3: Bidirectional ac/dc	
topology	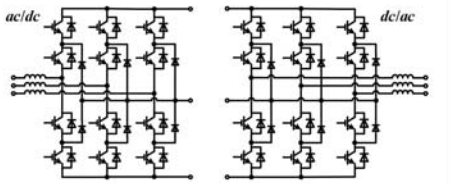	
cost (×$500)	C_3=2.4	
efficiency	η_3=0.975	
reliability	$R_3 = e^{-36\times10^{-6}t}$	

Fig. 12 *Topology and weights in terms of costs, efficiency, and reliability*

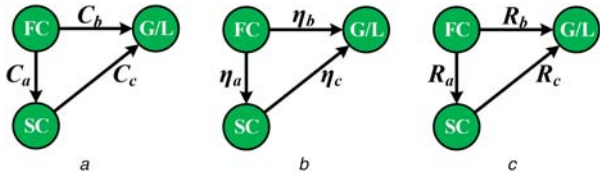

Fig. 13 *Evaluation models for architecture A.10*
(a) Cost model, ***(b)*** Efficiency model, ***(c)*** Reliability model

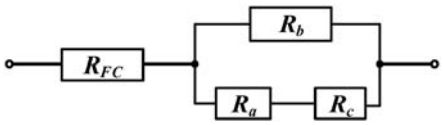

Fig. 14 *Reliability model of architecture A.10*

5.2 Case study

First, take the non-bus architecture A.10 as an example. The evaluation models in terms of costs, efficiency and reliability are presented in Fig. 13.

- Cost

  In the cost model shown in Fig. 13*a*, the weights of the edges are the costs of the corresponding converters. The total cost is the sum of the weights of all the edges. Therefore, the cost of the graph A.10 is shown in (13)

$$C_{\text{A.10}} = C_a + C_b + C_c = C_1 + C_1 + C_3 + C_1 + C_3 = 7.8, \tag{13}$$

  where C_1 and C_3 can be found in Fig. 12.

- Efficiency

  In the efficiency model shown in Fig. 13*b*, the weights of the edges are the efficiencies of the corresponding converters. Based on Fig. 13*b*, rewrite the weighted adjacency matrix, which is shown in (14)

Table 5 System parameters

Items	Values	Items	Values
FC	30 kW, 350–550 VMTBF: 3000 h	ac G/L	3 Phase; 220 V_{rms}; 50 Hz
SC	5.56 F135–250 V	dc-bus	750 V

Table 6 Converters selections for different edges

Edges	Converters	Edges	Converters
G/L→SC	ac/dc + buck dc/dc	SC→G/L	boost dc/dc + dc/ac
G/L↔SC	ac/dc + bi-dc/dc	FC→G/L	boost dc/dc + dc/ac
SC→FC	boost dc/dc	FC→SC	buck dc/dc
SC↔FC	bi-dc/dc	G↔bus	ac/dc
FC↔bus	bi-dc/dc	SC↔bus	bi-dc/dc

$$\boldsymbol{A}_{\text{A.10}} = \begin{bmatrix} 0 & \eta_a & \eta_b \\ 0 & 0 & \eta_c \\ 0 & 0 & 0 \end{bmatrix}. \tag{14}$$

The corresponding path matrix is presented in (15)

$$\boldsymbol{A}_{\text{A.10_T}} = \begin{bmatrix} 0 & \eta_a & \eta_b + \eta_a\eta_c \\ 0 & 0 & \eta_c \\ 0 & 0 & 0 \end{bmatrix}. \tag{15}$$

From (15), there are two paths from FC to G/L. The path with higher efficiency is selected to feeding the G/L as expressed in (16)

$$\eta_{\text{A.10_FC}\to\text{G/L}} = \eta_b = \eta_1\eta_3 = 0.946, \tag{16}$$

where η_1 and η_3 can be found in Fig. 12.

Similarly, the efficiency of the FC charging the SC can be obtained. From (15), the element (FC, SC) is η_a, and thus (17) is obtained

$$\eta_{\text{A.10_FC}\to\text{SC}} = \eta_a = \eta_1 = 0.97. \tag{17}$$

- Reliability

In the reliability model shown in Fig. 13*c*, the weights of the edges are the reliability of the corresponding converters. Based on Fig. 13*c*, rewrite the weighted adjacency matrix as presented in (18). Also, the path matrix is presented in (19)

$$\boldsymbol{A}_{\text{A.10}} = \begin{bmatrix} 0 & R_a & R_b \\ 0 & 0 & R_c \\ 0 & 0 & 0 \end{bmatrix}, \tag{18}$$

$$\boldsymbol{A}_{\text{A.10_T}} = \begin{bmatrix} 0 & R_a & R_b + R_aR_c \\ 0 & 0 & R_c \\ 0 & 0 & 0 \end{bmatrix}. \tag{19}$$

From (19), there are two paths from the FC to the G/L, and the reliability is R_b and R_aR_c, respectively. Therefore, the reliability model is obtained as presented in Fig. 14. Note that the reliability of the input source (FC) is included as well.

Based on Fig. 14, the reliability of the FC feeding the G/L is shown in (20)

$$\begin{aligned} R_{\text{A.10_FC}\to\text{G/L}} &= R_{\text{FC}}(1-(1-R_b)(1-R_aR_c)) \\ &= R_{\text{FC}}(1-(1-R_1R_3)(1-R_1R_1R_3)). \end{aligned} \tag{20}$$

Also, the reliability can be transformed into mean time between failure (MTBF). The result is shown in (21)

© The Institution of Engineering and Technology 2019
Page Page 7 of 11 (IPR2023-00758)
Netflix, Inc. v. GoTV Streaming, LLC

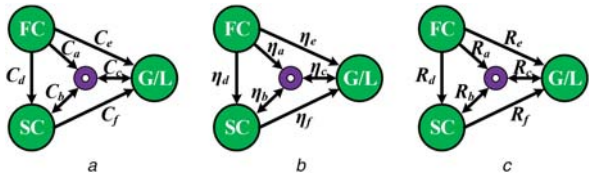

Fig. 15 *Evaluation models for architecture B.29*
(a) Cost model, ***(b)*** Efficiency model, ***(c)*** Reliability model

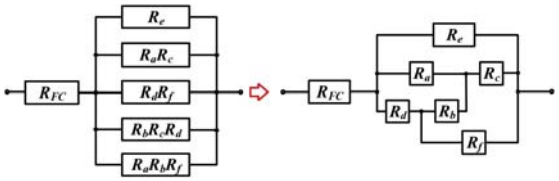

Fig. 16 *Reliability model of architecture B.29*

$$\mathrm{MTBF}_{\mathrm{A.10_FC\to G/L}}=\int_0^{\infty}R_{\mathrm{A.10_FC\to G/L}}(t)\,\mathrm{d}t=2636h\,. \quad (21)$$

There is another example presented in the following, which is based on the singular-bus architecture B.29. The evaluation models are presented in Fig. 15.

- Cost

  With the cost model shown in Fig. 15*a*, the cost of the architecture B.29 is shown in (22)

$$\begin{aligned}C_{\mathrm{B.29}}&=C_a+C_b+C_c+C_d+C_e+C_f\\&=4C_1+C_2+3C_3=12.4.\end{aligned} \quad (22)$$

- Efficiency

  Based on Fig. 15*b*, rewrite the weighted adjacency matrix as shown in (23)

$$\boldsymbol{A}_{\mathrm{B.29}}=\begin{bmatrix}0&\eta_d&\eta_e&\eta_a\\0&0&\eta_f&\eta_b\\0&0&0&\eta_c\\0&\eta_b&\eta_c&0\end{bmatrix}. \quad (23)$$

Based on (23), the corresponding path matrix can be obtained as well. The elements (FC, G/L) and (FC, SC) in the path matrix are shown in (24)

$$\begin{aligned}(\mathrm{FC,G/L})&=\eta_e+\eta_a\eta_c+\eta_d\eta_f+\eta_c\eta_b\eta_d+\eta_a\eta_b\eta_f,\\(\mathrm{FC,SC})&=\eta_d+\eta_a\eta_b+\eta_b\eta_c\eta_e\,.\end{aligned} \quad (24)$$

From (24), there are five paths from FC to G/L. The path with the highest efficiency is selected to feeding the G/L, which is expressed in (25)

$$\eta_{\mathrm{B.29_FC\to G/L}}=\eta_e=\eta_1\eta_3=0.946. \quad (25)$$

Similarly, the efficiency of the FC charging the SC can be obtained. From (25), the one with the highest efficiency is selected as shown in (26)

$$\eta_{\mathrm{B.29_FC\to SC}}=\eta_d=\eta_1=0.97. \quad (26)$$

- Reliability

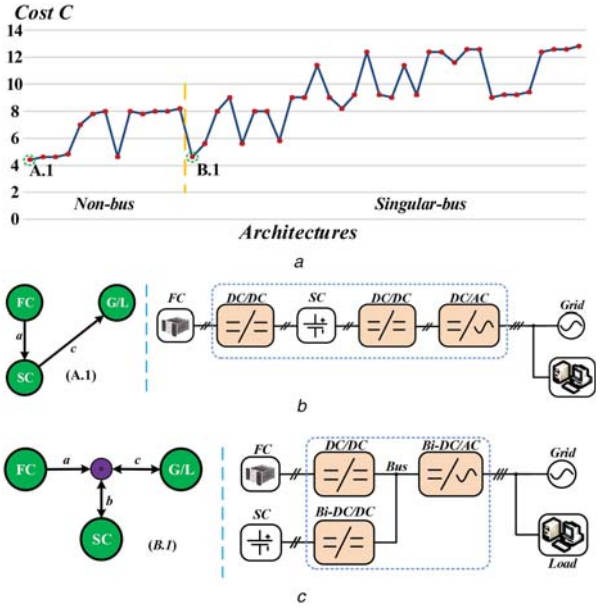

Fig. 17 *Results of costs for different architectures*
(a) Costs for different architectures, ***(b)*** Non-bus architecture with the lowest cost: A.1, ***(c)*** Singular-bus architecture with the lowest cost: B.1

Based on the reliability model shown in Fig. 15*c*, rewrite the weighted adjacency matrix as presented in (27)

$$\boldsymbol{A}_{\mathrm{B.27}}=\begin{bmatrix}0&R_d&R_e&R_a\\0&0&R_f&R_b\\0&0&0&R_c\\0&R_b&R_c&0\end{bmatrix}. \quad (27)$$

Based on (27), the corresponding path matrix can be obtained as well. The element (FC, G/L) in the path matrix is shown in (28)

$$\begin{aligned}(\mathrm{FC,G/L})&=R_e+R_aR_c+R_dR_f+R_cR_bR_d\\&\quad+R_aR_bR_f\,.\end{aligned} \quad (28)$$

From (28), there are five paths from the FC to the G/L. Therefore, the reliability model is obtained as presented in Fig. 16.

Based on Fig. 16, the reliability of the FC feeding the G/L is shown in (29) (see (29)) . Also, the reliability can be transformed into MTBFs as shown in (30)

$$\begin{aligned}\mathrm{MTBF}_{\mathrm{B.29_FC\to G/L}}&=\int_0^{\infty}R_{\mathrm{B.29_FC\to G/L}}(t)\,\mathrm{d}t\\&=2833h\,.\end{aligned} \quad (30)$$

Following the same method, the results for all the deduced architectures can be obtained. Fig. 17*a* presents the costs for different architectures. From it, among the non-bus architectures, the architecture A.1 has the lowest cost. For the singular-bus architectures, the cost of the architecture B.1 is the lowest. Also, these two architectures are shown in Figs. 17*b* and *c*, respectively.

The efficiency of the FC feeding the G/L ($\eta_{\mathrm{FC\to G/L}}$) is presented in Fig. 18. From it, most of the architectures can achieve high efficiency (94.6%) when the FC powers the G/L. However,

$$\begin{aligned}R_{\mathrm{B.29_FC\to G/L}}&=R_aR_bR_cR_dR_e-R_aR_bR_cR_dR_eR_f+R_dR_f+R_e-R_dR_eR_f\\&\quad+R_bR_cR_d-R_bR_cR_dR_f-R_bR_cR_dR_e+R_bR_cR_dR_eR_f+R_aR_c-R_aR_cR_dR_f\\&\quad-R_aR_cR_e+R_aR_cR_dR_eR_f-R_aR_bR_cR_d+R_aR_bR_cR_dR_f+R_aR_bR_cR_dR_e\\&\quad+R_aR_bR_cR_dR_eR_f\,.\end{aligned} \quad (29)$$

© The Institution of Engineering and Technology 2019
Page Page 8 of 11 (IPR2023-00758)
Netflix, Inc. v. GoTV Streaming, LLC

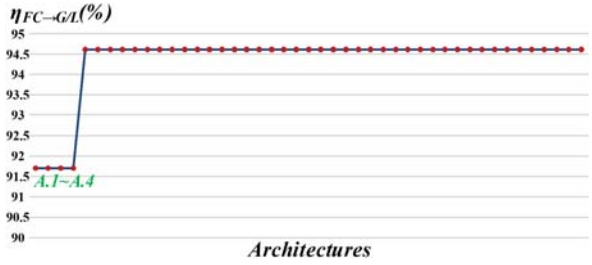

Fig. 18 *Results of FC→G/L efficiency for different architectures*

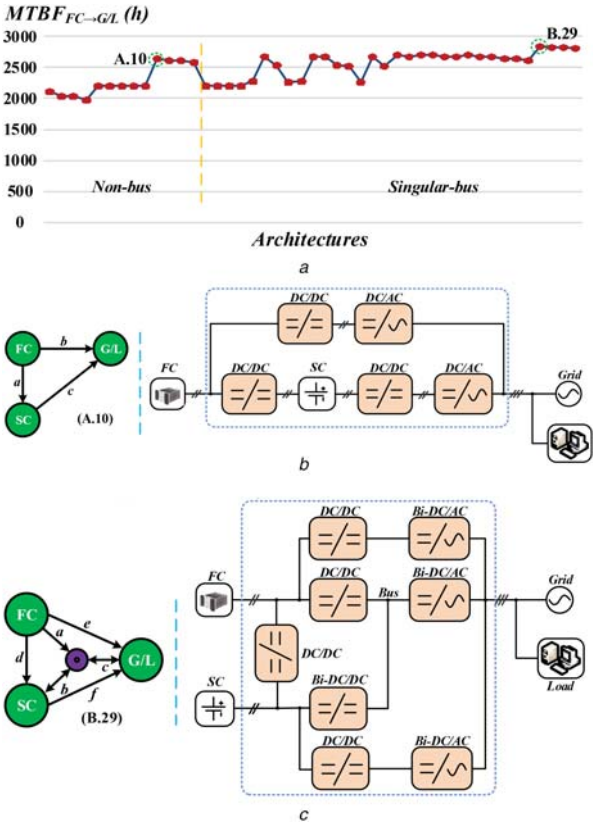

Fig. 19 *Results of the FC→G/L reliability for different architectures*
(a) MTBFs for different architectures, ***(b)*** High reliability non-bus architecture A.10, ***(c)*** High reliability singular-bus architecture B.29

the efficiency of the architectures, including A.1, A.2, A.3, and A.4, is relatively low (91.7%) compared with other architectures.

The reliability of the FC feeding the G/L for different architectures is presented in Fig. 19. From it, among the non-bus architectures, the architecture A.10 has the highest reliability, where the MTBF is 2636 h. For the singular-bus architectures, the reliability of the architecture B.29 is the highest, and the corresponding MTBF is 2833 h. Also, the architectures of A.10 and B.29 are shown in Figs. 19*b* and *c*, respectively.

To find a compromise among costs, efficiency, and reliability, multiple objective optimisation is applied. First, a nominalisation is introduced as shown in (31)

$$\begin{cases} C' = \dfrac{C}{C_{\max}}, \\ \eta'_{\mathrm{FC}\rightarrow \mathrm{G/L}} = \dfrac{\eta_{\mathrm{FC}\rightarrow \mathrm{G/L}}}{\eta_{\max}}, \\ \mathrm{MTBF}'_{\mathrm{FC}\rightarrow \mathrm{G/L}} = \dfrac{\mathrm{MTBF}_{\mathrm{FC}\rightarrow \mathrm{G/L}}}{\mathrm{MTBF}_{\max}}, \end{cases} \tag{31}$$

where $C_{\max}$ is 12.8, $\eta_{\max}$ is 0.946, and $\mathrm{MTBF}_{\max}$ is 2833.

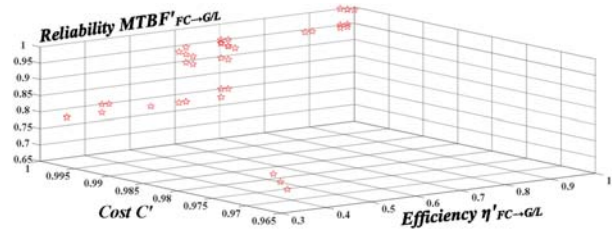

Fig. 20 *Results of C', $\eta'_{FC\rightarrow G/L}$ and $MTBF'_{FC\rightarrow G/L}$ for different architectures*

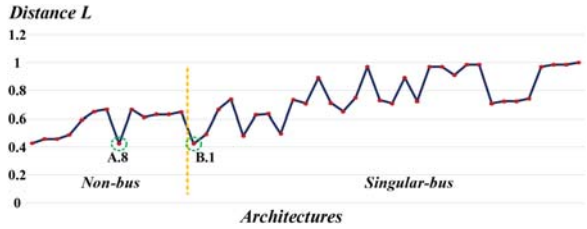

Fig. 21 *Distance L for different architectures*

With (31), the results of C', $\eta'_{\mathrm{FC}\rightarrow \mathrm{G/L}}$, and $\mathrm{MTBF}'_{\mathrm{FC}\rightarrow \mathrm{G/L}}$ for different architectures are obtained and plotted in Fig. 20.

The ideal architecture is that $C' = 0$, $\eta'_{\mathrm{FC}\rightarrow \mathrm{G/L}} = 1$ and $\mathrm{MTBF}'_{\mathrm{FC}\rightarrow \mathrm{G/L}} = 1$. Thus, calculate the distance from the architecture candidates to the ideal architecture. The expression is shown in (32)

$$L = \sqrt{(C'-0)^2 + (\eta'_{\mathrm{FC}\rightarrow \mathrm{G/L}} - 1)^2 + (\mathrm{MTBF}'_{\mathrm{FC}\rightarrow \mathrm{G/L}} - 1)^2}. \tag{32}$$

The distances L for different architectures are calculated and presented in Fig. 21. The one with the shortest distance is considered the best architecture compromise. From Fig. 21, the non-bus architecture A.8 and the singular-bus architecture B.1 have the shortest distance L. Therefore, these two architectures are considered the best architecture compromise for the demo system. Also, with the consideration of the fact that the bus-structures are easier to control compared with non-bus structures, the architecture B.1 is chosen for the experimental platform.

6 Experimental results

A 30 kW FC experimental platform is built and the dc-bus architecture B.1 is selected. Fig. 22*a* presents the communication and control architecture for the system. Also, the topology of the system is shown in Fig. 22*b*.

The parameters of the system are presented in Table 7.

The basic function of the system is to provide high-quality power to the output in both stand-alone mode (see Fig. 23*a*) and grid-connected mode (see Fig. 23*b*). Figs. 23*c* and *d* show the experimental results in the stand-alone mode and the grid-connected mode. From these figures, the system can feed both high-quality voltage to the load and high-quality current to the grid.

Fig. 24*a* presents the total harmonic distortions (THDs) of the load voltage and the grid current. From it, the goal that the load voltage THD is <3% and the grid-current THD at the rated power is <5% can be satisfied. Furthermore, the system efficiency from the FC to the output is 94.1% at the rated power as shown in Fig. 24*b*, which is much higher than the traditional boost plus two-level structure [9].

Fig. 25 presents the transition from the stand-alone mode at 3 kW to the grid-connected mode at 27 kW. From Fig. 25*a*, after the grid is connected, the system is switched from a voltage source to a current source. Then, the current reference is increased gradually until the output power reaches the target. From Fig. 25*b*, the whole transition process is seamless and there are not any voltage or current surges during the transition. Also, the load voltage is uninterrupted during the transition.

© The Institution of Engineering and Technology 2019
Page Page 9 of 11 (IPR2023-00758)
Netflix, Inc. v. GoTV Streaming, LLC

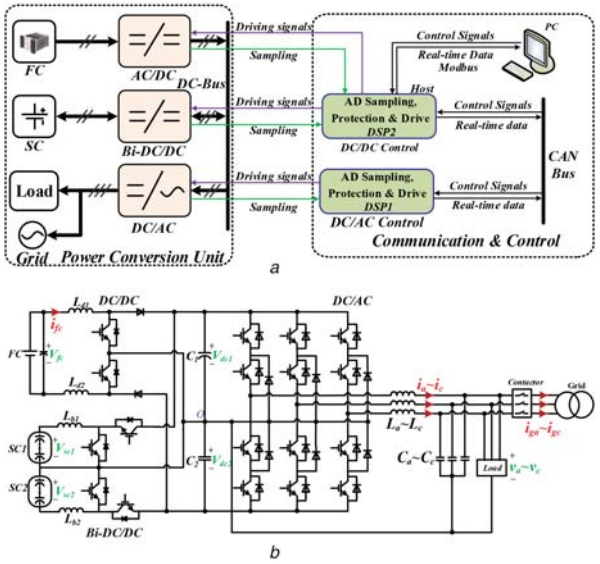

Fig. 22 *System communication architecture and topology*
(a) Communication and control architecture, ***(b)*** Topology

Table 7 Parameters of the system

Item	Value	Item	Value
rated power	30 kW	switching frequency	10 kHz
FC voltage (V_{fc})	350–550 V	dc/dc inductance (L_{d1}–L_{d2})	0.16 mH
dc-bus voltage (V_{dc1}–V_{dc2})	375 V	SC voltage (V_{sc1}–V_{sc2})	135–250 V
SC inductance (C_{sc1}–C_{sc2})	5.56 F	bi-dc/dc inductance (L_{b1}–L_{b2})	0.16 mH
G/L	220 V_{rms}50 Hz	dc/ac capacitance (C_a–C_c)	25 μF
dc/ac inductance (L_a–L_c)	0.5 mH	—	—

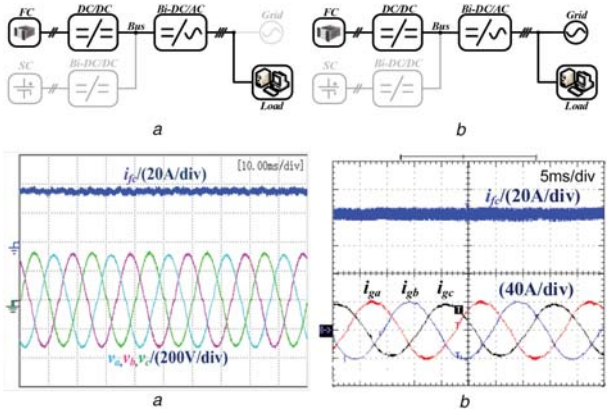

Fig. 23 *Experimental results in two modes*
(a) Stand-alone mode, ***(b)*** Grid-connected mode, ***(c)*** Stand-alone mode (15 kW), ***(d)*** Grid-connected mode (24 kW)

Fig. 26 presents the transition from the grid-connected mode at 27 kW to the stand-alone mode at 3 kW. From Fig. 25*a*, after the grid is disconnected, the system is quickly switched to a voltage source from a current source. Thus, the load voltage can be maintained. From Fig. 26*b*, the whole transition process is seamless and there are not any voltage or current surges during the transition.

The function of the SC in the system is to compensate for the slow dynamics of the FC in cases of load changes (see Fig. 27*a*).

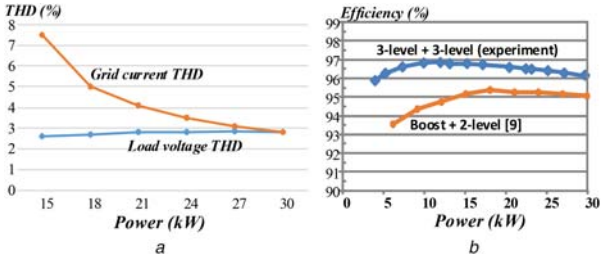

Fig. 24 *THDs and efficiency of the system*
(a) THDs, ***(b)*** Efficiency

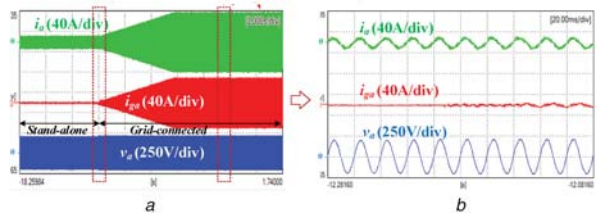

Fig. 25 *Transition from stand-alone to grid-connected*
(a) Whole process, ***(b)*** Transition moment

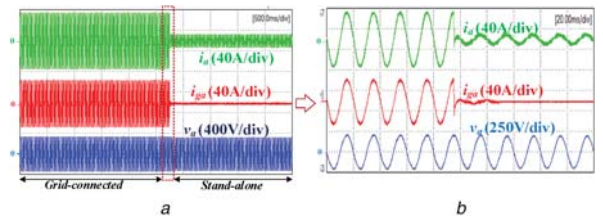

Fig. 26 *Transition from grid-connected to stand-alone*
(a) Whole process, ***(b)*** Transition moment

Figs. 27*b* and *c* present the experimental results when the output power steps up and steps down. Since the SC can provide dynamic power, the FC power can slowly change as shown in Figs. 27*b* and *c*. Therefore, the change rate of the FC power is limited with the help of the SCs and the lifespan of the FC can be extended.

7 Conclusions

This study proposes a systematic approach to construct and evaluate PCAs using graph theory. First, the graph model for the components in PCSs is built, where five types of components are modelled as either nodes or edges. Then, based on the adjacency matrices, the processes of adding extra edges and buses to deduce possible PCAs are mathematically detailed. For the FC demo system, 13 non-bus architectures and 32 singular-bus architectures are generated with the proposed methodology. Furthermore, the proposed methodology of searching possible PCAs is a generalised approach and can be applied in complex systems with any number of nodes. Also, an evaluation methodology based on graph theory is proposed to find the best architecture compromise in terms of costs, efficiency, and reliability. For the FC demo system, with the proposed assessment methodology, the best architecture compromises are found among 45 possible architectures. From the analysis, the proposed PCA construction and assessment method is based on mathematical deductions and can be easily implemented via software computing, which makes it possible to find the optimised PCAs for large-scale PCSs. Finally, the experimental platform is built, where the dc-bus optimised architecture is adopted, and the experimental results show the architecture selection can fulfil the system requirements.

8 Acknowledgment

The author thanks Zhejiang University for experiment support of this work during the Ph.D. study.

© The Institution of Engineering and Technology 2019

Page Page 10 of 11 (IPR2023-00758)
Netflix, Inc. v. GoTV Streaming, LLC

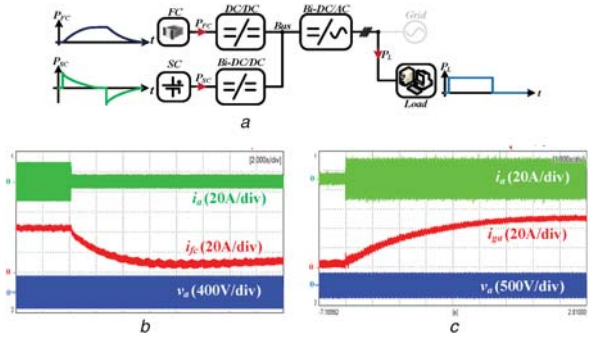

Fig. 27 *FC dynamic compensation in cases of the load changes*
(a) SC compensates FC's slow dynamics, ***(b)*** 15–3 kW, ***(c)*** 3–15 kW

9 References

[1] Zhang, W., Xu, D., Enjeti, P.N., *et al.*: 'Survey on fault-tolerant techniques for power electronic converters', *IEEE Trans. Power Electron.*, 2014, **29**, (12), pp. 6319–6331

[2] Chen, Z., Guerrero, J.M., Blaabjerg, F.: 'A review of the state of the art of power electronics for wind turbines', *IEEE Trans. Power Electron.*, 2009, **24**, (8), pp. 1859–1875

[3] Dragičević, T., Lu, X., Vasquez, J.C., *et al.*: 'DC microgrids – part II: a review of power architectures, applications, and standardization issues', *IEEE Trans. Power Electron.*, 2016, **31**, (5), pp. 3528–3549

[4] Liu, X., Wang, P., Loh, P.C.: 'A hybrid AC/DC microgrid and its coordination control', *IEEE Trans. Smart Grid*, 2011, **2**, (2), pp. 278–286

[5] Zhang, W., Xu, D., Li, X., *et al.*: 'Seamless transfer control strategy for fuel cell uninterruptible power supply system', *IEEE Trans. Power Electron.*, 2013, **28**, (2), pp. 717–729

[6] Lindman, P., Thorsell, L.: 'Applying distributed power modules in telecom systems', *IEEE Trans. Power Electron.*, 1996, **11**, (2), pp. 365–373

[7] Balog, R.S., Krein, P.T.: 'Bus selection in multibus DC microgrids', *IEEE Trans. Power Electron.*, 2011, **26**, (3), pp. 860–867

[8] Choung, S.H., Kwasinski, A.: 'Multiple-input DC-DC converter topologies comparison'. 2008 34th Annual Conf. of IEEE Industrial Electronics, Orlando, FL, 2008, pp. 2359–2364

[9] Li, X., Zhang, W., Du, C., *et al.*: 'Investigation to power conversion topology for fuel cell power generation system'. 2010 Int. Power Electronics Conf. – ECCE ASIA, Sapporo, 2010, pp. 2637–2643

[10] Xu, D., Li, H., Zhu, Y., *et al.*: 'High-surety microgrid: super uninterruptable power supply with multiple renewable energy sources', *Electr. Power Compon. Syst.*, 2015, **43**, (8–10), pp. 839–853

[11] Shi, K., Li, H., Hu, C., *et al.*: 'Topology of super uninterruptible power supply with multiple energy sources'. 2015 9th Int. Conf. on Power Electronics and ECCE Asia (ICPE-ECCE Asia), Seoul, 2015, pp. 1742–1749

[12] Hernandez-Aramburo, C.A., Green, T.C., Mugniot, N.: 'Fuel consumption minimization of a microgrid', *IEEE Trans. Ind. Appl.*, 2005, **41**, (3), pp. 673–681

[13] Kwasinski, A.: 'Quantitative evaluation of DC microgrids availability: effects of system architecture and converter topology design choices', *IEEE Trans. Power Electron.*, 2011, **26**, (3), pp. 835–851

[14] Lefranc, P., Jannot, X., Dessante, P.: 'Virtual prototyping and pre-sizing methodology for buck DC-DC converters using genetic algorithms', *IET Power Electron.*, 2012, **5**, (1), pp. 41–52

[15] Chen, S.X., Gooi, H.B.: 'Jump and shift method for multi-objective optimization', *IEEE Trans. Ind. Electron.*, 2011, **58**, (10), pp. 4538–4548

[16] Marxgut, C., Muhlethaler, J., Krismer, F., *et al.*: 'Multiobjective optimization of ultraflat magnetic components with PCB-integrated core', *IEEE Trans. Power Electron.*, 2013, **28**, (7), pp. 3591–3602

[17] Andersen, T.M., Zingerli, C.M., Krismer, F., *et al.*: 'Modeling and Pareto optimization of microfabricated inductors for power supply on chip', *IEEE Trans. Power Electron.*, 2013, **28**, (9), pp. 4422–4430

[18] Schrittwieser, L., Kolar, J.W., Soeiro, T.B.: '99% efficient three-phase buck-type SiC MOSFET PFC rectifier minimizing life cycle cost in DC data centers', *CPSS Trans. Power Electron. Appl.*, 2017, **2**, (1), pp. 47–58

[19] Bjeletić, A., Corradini, L., Maksimović, D., *et al.*: 'Specifications-driven design space boundaries for point-of-load converters'. 2011 Twenty-Sixth Annual IEEE Applied Power Electronics Conf. and Exposition (APEC), Fort Worth, TX, 2011, pp. 1166–1173

[20] Boillat, D.O., Krismer, F., Kolar, J.W.: 'Design space analysis and ρ-η Pareto optimization of LC output filters for switch-mode AC power sources', *IEEE Trans. Power Electron.*, 2015, **30**, (12), pp. 6906–6923

[21] Burkart, R.M., Kolar, J.W.: 'Comparative life cycle cost analysis of Si and SiC PV converter systems based on advanced η–ρ–σ multiobjective optimization techniques', *IEEE Trans. Power Electron.*, 2017, **32**, (6), pp. 4344–4358

[22] Deblecker, O., Versèle, C., De Grève, Z., *et al.*: 'Multiobjective optimization of a power supply for space application using a flexible CAD tool'. 2013 15th European Conf. on Power Electronics and Applications (EPE), Lille, 2013, pp. 1–10

[23] Kolar, J.W., Friedli, T., Krismer, F., *et al.*: 'Conceptualization and multiobjective optimization of the electric system of an airborne wind turbine', *IEEE J. Emerging Sel. Topics Power Electron.*, 2013, **1**, (2), pp. 73–103

[24] Burkart, R.M., Kolar, J.W.: 'Comparative η–ρ–σ Pareto optimization of Si and SiC multilevel dual-active-bridge topologies with wide input voltage range', *IEEE Trans. Power Electron.*, 2017, **32**, (7), pp. 5258–5270

[25] Sayeekumar, N., Ahmed, K. S., Karthikeyan, S.P., *et al.*: 'Graph theory and its applications in power systems – a review'. 2015 Int. Conf. on Control, Instrumentation, Communication and Computational Technologies (ICCICCT), Kumaracoil, 2015, pp. 154–157

[26] Chai, S., Sekar, A.: 'Graph theory application to deregulated power system'. Proc. 33rd Southeastern Symp. on System Theory, Athens, OH, 2001, pp. 117–121

[27] Xie, N., Torelli, F., Bompard, E., *et al.*: 'A graph theory based methodology for optimal PMUs placement and multiarea power system state estimation', *Electr. Power Syst. Res.*, 2015, **119**, pp. 25–33

[28] Garg, R.K., Agrawal, V.P., Gupta, V.K.: 'Selection of power plants by evaluation and comparison using graph theoretical methodology', *Int. J. Electr. Power Energy Syst.*, 2006, **28**, (6), pp. 429–435

[29] Košťálová, A., Carvalho, P.: 'Towards self-healing in distribution networks operation: bipartite graph modelling for automated switching', *Electr. Power Syst. Res.*, 2011, **81**, (1), pp. 51–56

[30] Smedley, K., Cuk, S.: 'Switching flow-graph nonlinear modeling technique', *IEEE Trans. Power Electron.*, 1994, **9**, (4), pp. 405–413

[31] Zhang, B., Qiu, D.: 'Sneak circuits in power converters: concept, principle and application', *CPSS Trans. Power Electron. Appl.*, 2017, **2**, (1), pp. 68–75

[32] Li, X., Zhang, W., Li, H., *et al.*: 'Power management unit with its control for a three-phase fuel cell power system without large electrolytic capacitors', *IEEE Trans. Power Electron.*, 2011, **26**, (12), pp. 3766–3777

© The Institution of Engineering and Technology 2019
Page Page 11 of 11 (IPR2023-00758)
Netflix, Inc. v. GoTV Streaming, LLC